

Appearance and disappearance of quantum correlations in measurement-based feedback control of a mechanical oscillator

V. Sudhir,¹ D.J. Wilson,¹ R. Schilling,¹ H. Schütz,¹ S.A. Fedorov,¹
A.H. Ghadimi,¹ A. Nunnenkamp,² and T.J. Kippenberg¹

¹*Institute for Condensed Matter Physics, École Polytechnique Fédérale de Lausanne, Lausanne 1015, Switzerland*

²*Cavendish Laboratory, University of Cambridge, Cambridge CB3 0HE, United Kingdom*

(Dated: February 19, 2024)

Quantum correlations between imprecision and back-action are a hallmark of continuous linear measurements. Here we study how measurement-based feedback can be used to improve the visibility of quantum correlations due to the interaction of a laser field with a nano-optomechanical system. Back-action imparted by the meter laser, due to radiation pressure quantum fluctuations, gives rise to correlations between its phase and amplitude quadratures. These quantum correlations are observed in the experiment both as squeezing of the meter field fluctuations below the vacuum level in a homodyne measurement, and as sideband asymmetry in a heterodyne measurement, demonstrating the common origin of both phenomena. We show that quantum feedback, i.e. feedback that suppresses measurement back-action, can be used to increase the visibility of the sideband asymmetry ratio. In contrast, by operating the feedback loop in the regime of noise squashing, where the in-loop photocurrent variance is reduced below the vacuum level, the visibility of the sideband asymmetry is reduced. This is due to feedback back-action arising from vacuum noise in the homodyne detector. These experiments demonstrate the possibility, as well as the fundamental limits of measurement-based feedback as a tool to manipulate quantum correlations.

Measurements proceed by establishing correlations between a system and a meter. In a quantum description of this process [1], the effect of measurement persists in the system in the form of measurement back-action. For continuous linear measurement [2, 3], where the meter couples linearly and weakly to the system, correlations between the system and meter additionally manifest as back-action-induced quantum correlations between the degrees of freedom of the meter. A paradigmatic example is the interferometric position readout of a mechanical oscillator [4]. The meter in this case is an optical field, which possesses two degrees of freedom (quadratures): amplitude and phase. The position of the oscillator is imprinted onto the phase quadrature. Back-action arises from vacuum fluctuations of the amplitude quadrature, which are imprinted onto the phase via the back-action-driven motion of the oscillator, leading to amplitude-phase quantum correlations in the meter field. In a homodyne detector, these quantum correlations manifest as ponderomotive squeezing of an appropriately chosen field quadrature [5–8]. In a heterodyne detector, they manifest as motional sideband asymmetry [9–12]. Differences between these effects arise from the details of how meter fluctuations are converted to a classical signal by the detection process [10, 13–15] [16]

Here we investigate the effect of measurement-based feedback on quantum correlations due to the interaction of an optical field with a nano-mechanical oscillator. Recent advances [17] have enabled operation of an optomechanical system such that the mechanical oscillator can be measured at a rate approaching the thermal decoherence rate, a regime where measurement back-action becomes relevant compared to the thermal noises. Harnessing this capability, here we show that feedback of a homodyne measurement can be used to improve the

visibility of motional sideband asymmetry by suppressing measurement back-action. Indeed, the feedback loop cools the oscillator to a final phonon occupancy (n_{eff}) that is more than two orders of lower than that due to the quantum backaction (n_{qba}) of the meter beam. The system therefore operates in the *quantum feedback* regime, where quantum back-action is effectively suppressed by feedback, and feedback can manipulate quantum correlations without destroying them. This is possible because the measurement used for feedback contains a faithful record of its own back-action [18]. Further we study how these quantum correlations are obscured in the regime where feedback is dominated by quantum noise in the in-loop detector (i.e. feedback back-action); a regime giving rise to “squashing” of the in-loop photocurrent [19]. This demonstrates the complementary scenario where feedback is detrimental to the observation of quantum correlations. Conceptually, this feedback back-action dominated regime is analogous to the quantum back-action limit of sideband cooling [20]. Finally, we probe quantum correlations via a homodyne detector tuned close to the amplitude quadrature, and observe squeezing, i.e. a reduction of the homodyne noise below the vacuum level. By observing both squeezing and sideband asymmetry in the same device, the common origin of motional sideband asymmetry [10, 14] and optical squeezing [8, 11] in general dyne detection [1] of the meter field is experimentally illustrated.

A pedagogical description of continuous linear measurement is germane to understanding our approach. We denote as $x(t)$ the position of a quantum harmonic oscillator and $y(t) \propto x(t)$ the output of a linear continuous position detector. Since it is a continuous observable, $y(t)$ must commute with itself at different times ($[y(t), y(t')] = 0$). $x(t)$ does not obey this constraint,

which requires that the detector output contains an additional noise term $x_n(t)$ that enforces the commutator. x_n contains two components: an apparent (imprecision) noise, x_{imp} , which arises from quantum fluctuations of the meter degree of freedom that is coupled to the detector, and a physical (back-action) noise, x_{ba} , which arises from quantum fluctuations of the meter degree of freedom that is coupled to the system. The total detector signal, $y = x + x_{\text{ba}} + x_{\text{imp}} \equiv x_{\text{tot}} + x_{\text{imp}}$, is characterized by a (symmetrized, double-sided [21]) noise spectrum [3, 22],

$$\bar{S}_{yy}(\Omega) = \bar{S}_{xx}^{\text{imp}}(\Omega) + \bar{S}_{xx}^{\text{tot}}(\Omega) + 2\text{Re} \bar{S}_{x_{\text{ba}}x_{\text{imp}}}(\Omega), \quad (1)$$

which contains terms due to quantum fluctuations of the meter (x_{imp}), total physical motion (x_{tot}), and quantum (imprecision-back-action) correlations, respectively.

In our experiment we monitor the position fluctuations of a cryogenically pre-cooled ($T \approx 6$ K) nanomechanical string coupled dispersively to an optical microcavity [23]. The fundamental mode of the string forms the oscillator (frequency $\Omega_m = 2\pi \cdot 4.3$ MHz, damping rate $\Gamma_m = 2\pi \cdot 7$ Hz). The meter is a laser field passing resonantly through the cavity (wavelength, $\lambda \approx 774$ nm), whose quadratures are monitored simultaneously by a homodyne and a heterodyne detector (Fig. 1a). Both detectors are operated with an imprecision far below that at the SQL, implying that quantum back-action due to the measurement (quantified as a phonon occupancy n_{qba}) is a significant contribution to the total motion of the nanomechanical oscillator (n_{tot}), i.e., $n_{\text{qba}} \approx 0.15 n_{\text{tot}}$.

We first assess the resulting optomechanical quantum correlations by measuring the output field in a homodyne detector. Measuring the quadrature of the meter field at phase θ , imprecision-back-action correlations in a homodyne detector take the form [22],

$$\bar{S}_{x_{\text{ba}}x_{\text{imp}}}^{\text{hom}}(\Omega) \propto C\eta_{\text{hom}} \sin(2\theta)\chi_m(\Omega), \quad (2)$$

where $C = 4g_0^2 n_c / \kappa \Gamma_m$ is the multi-photon cooperativity of the optomechanical system, η_{hom} is the detection efficiency and $\chi_m(\Omega) = (-\Omega^2 + \Omega_m^2 - i\Omega\Gamma_m)^{-1}/m$ is the susceptibility of the mechanical oscillator to an applied force. In the phase quadrature ($\theta = \pi/2$), where sensitivity to mechanical motion is largest (shown in Fig. 1b top left), these correlations do not appear in the homodyne photocurrent. However, near the amplitude quadrature, $\theta \rightarrow 0$, the magnitude of the correlation term can be comparable to the thermal motion, leading to observable squeezing of the homodyne photocurrent [24]. Fig. 2 shows homodyne detection of optical squeezing near the amplitude quadrature. The observed squeezing, while small in magnitude 1%, can still be clearly observed in the measurement.

Detecting ponderomotive squeezing provides bona fide proof of the presence of quantum correlations in the meter field. We next probe the alternate manifestation of these correlations as sideband asymmetry – in a heterodyne detector. The heterodyne detector used in the experiment monitors both quadratures of the meter simultaneously [22], giving access to $\bar{S}_{yy}^{\text{het}}(\Omega > 0)$, where

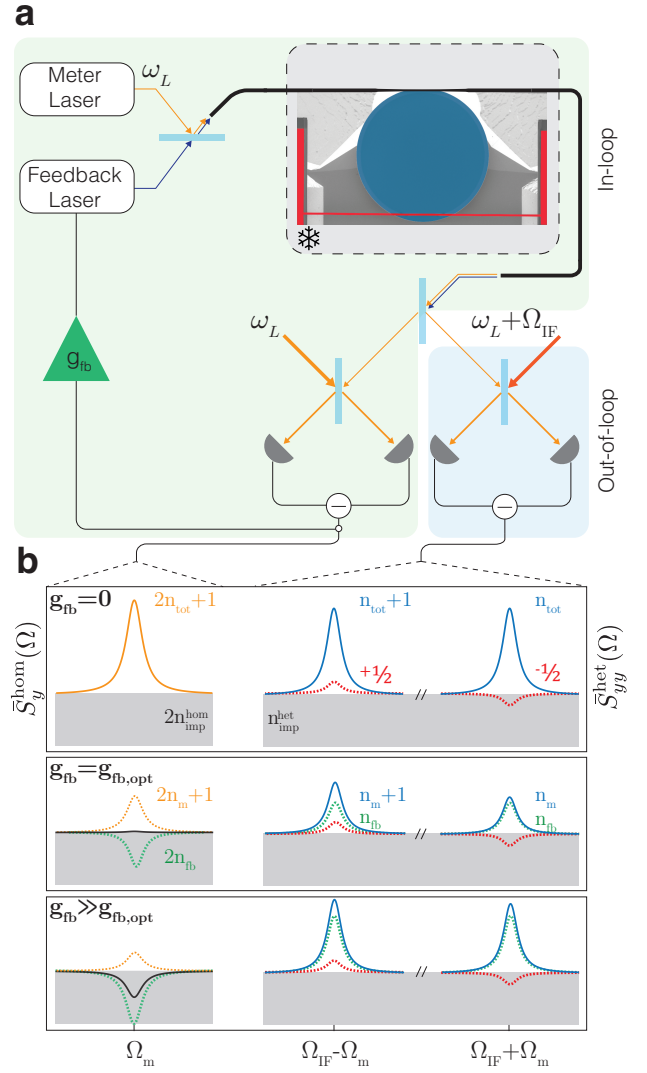


FIG. 1. Using homodyne feedback to increase the visibility of quantum-correlation-induced motional sideband asymmetry. (a) Linear position measurement and feedback control of a nanomechanical string (Si_3N_4 , red) is provided by evanescent coupling to an optical microdisk cavity (SiO_2 , blue). Whispering gallery modes of the microdisk are driven by a pair of tunable diode lasers using a tapered optical fiber (black). The ‘meter’ field (orange) is directed to a pair of balanced interferometers (homodyne, green; heterodyne, blue). A delayed and an amplified copy of the homodyne signal is imprinted onto the amplitude of the ‘feedback’ field (blue), effecting cold damping of the fundamental beam mode. Taper, nanobeam, and microdisk are integrated into a He cryostat (grey). (b) Schematic of the closed-loop homodyne (left) and heterodyne (right) noise spectrum for various feedback gains. Contributions from measurement imprecision, physical motion, and imprecision-back-action correlations are delineated by color.

$\bar{S}_{yy}^{\text{het}}(\Omega_{\text{IF}} \pm \Omega_m)$ correspond to upper (+) and lower (−) motional sidebands (displaced by the heterodyne intermediate frequency, Ω_{IF}). Quantum correlations between the phase and amplitude of the meter manifest as an

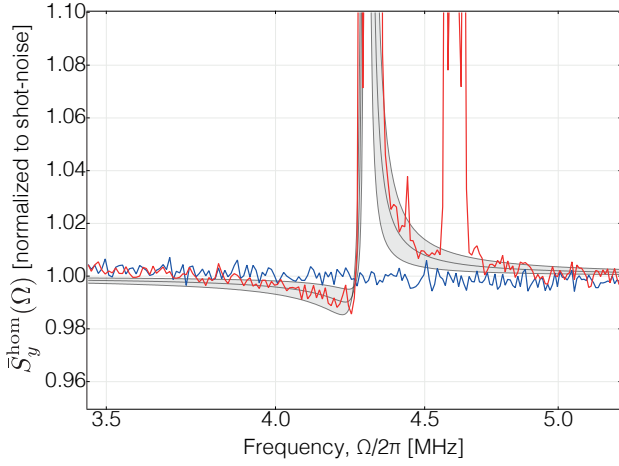


FIG. 2. **Squeezing in homodyne detection.** Quantum correlations in the cavity transmission manifest as photocurrent squeezing when measured using a homodyne detector set to near the amplitude quadrature (here $\theta \approx 0.1$ rad). Blue trace shows the shot-noise in the homodyne detector when the meter field is in vacuum. Red shows measurement when the meter field has interacted with the mechanical oscillator; squeezing at the level of 1% is visible, consistent with theoretical predictions (black) using a model incorporating $\approx 5\%$ uncertainties (gray regions) in the experimentally measured system parameters. The wideband shot noise detected far from mechanical resonance agrees very well with the expected local oscillator shot noise. By directing all of the cavity transmission to the homodyne detector, we realize an overall detection efficiency, $\eta_{\text{hom}} \approx 0.2$.

asymmetry of the heterodyne motional sidebands. This can be understood from the three terms in Eq. (1), illustrated as components of the heterodyne signal in Fig. 1b (top right panel). Detector imprecision (gray) – arising from the vacuum fluctuations in the phase and amplitude quadrature of the probe – contributes a phonon-equivalent noise of $n_{\text{imp}}^{\text{het}} \equiv \bar{S}_{yy}^{\text{het,imp}}(\Omega_{\text{IF}} \pm \Omega_m) / \bar{S}_{xx}^{\text{zp}}(\Omega_m)$. Physical motion – arising from a combination of thermal force and meter back-action – contributes $n_m + \frac{1}{2}$ phonons to each sideband. Imprecision-back-action correlations – arising from amplitude-phase correlations in the meter – contribute $\pm \frac{1}{2}$ phonons to the lower/upper sideband (red dashed) [22], where $\bar{S}_{xx}^{\text{zp}}(\Omega_m) = \frac{4x_{\text{zp}}^2}{\Gamma_m}$ is the zero-point position spectral density on resonance. The resulting asymmetry of the sidebands (blue traces),

$$R \equiv \frac{\bar{S}_{yy}^{\text{het}}(\Omega_{\text{het}}^+) - \bar{S}_{yy}^{\text{het,imp}}(\Omega_{\text{het}}^+)}{\bar{S}_{yy}^{\text{het}}(\Omega_{\text{het}}^-) - \bar{S}_{yy}^{\text{het,imp}}(\Omega_{\text{het}}^-)} \approx \frac{n_m}{n_m + 1}, \quad (3)$$

is commensurate with one phonon and arises purely from quantum correlations in the meter (here $\Omega_{\text{het}}^{\pm} \equiv \Omega_{\text{IF}} \pm \Omega_m$). This asymmetry corresponds directly to the visibility of imprecision-back-action correlations with respect to the total noise power, i.e.,

$$\xi \equiv \frac{2\text{Re } \bar{S}_{x_{\text{ba}}x_{\text{imp}}}(\Omega_{\text{het}}^+)}{\bar{S}_{xx}^{\text{imp}}(\Omega_{\text{het}}^+) + S_{xx}^{\text{tot}}(\Omega_{\text{het}}^+)} \approx \frac{1 - R}{1 + R} = \frac{1}{2n_m + 1}. \quad (4)$$

Our objective is to increase the sideband asymmetry $1 - R$ in the heterodyne spectrum, and thereby ξ , by actively cold damping [17, 25] the mechanical oscillator using the homodyne measurement as an error signal. Concretely, the homodyne signal in the phase quadrature ($\theta = \pi/2$) is imprinted onto the amplitude quadrature of an independent *feedback* laser resonant with an auxiliary cavity mode ($\lambda \approx 840$ nm). The loop delay is tuned in order to produce a purely viscous radiation pressure feedback force, effectively coupling the oscillator at a rate $\Gamma_{\text{fb}} \approx g_{\text{fb}}\Gamma_m$ to a cold bath with an occupation equal to the phonon-equivalent homodyne imprecision $n_{\text{imp}}^{\text{hom}} = \bar{S}_x^{\text{imp,hom}}(\Omega_m) / 2\bar{S}_x^{\text{zp}}(\Omega_m)$ (here g_{fb} is the dimensionless gain of the feedback loop). The occupation of the oscillator is thereby reduced to,

$$n_m + \frac{1}{2} \approx \frac{n_{\text{tot}}}{g_{\text{fb}}} + g_{\text{fb}}n_{\text{imp}}^{\text{hom}} \geq 2\sqrt{n_{\text{tot}}n_{\text{imp}}^{\text{hom}}}, \quad (5)$$

with the minimum achieved at an optimal gain of $g_{\text{fb}}^{\text{opt}} = \sqrt{n_{\text{tot}}/n_{\text{imp}}^{\text{hom}}}$. (Here, $n_{\text{tot}} = n_{\text{th}} + n_{\text{ba}}$ is the effective bath occupation of the mechanical oscillator, including measurement back-action.) Notably, cold-damping allows access to $n_m \rightarrow 0$ when a highly efficient measurement is used, corresponding to an imprecision-back-action product approaching the uncertainty limit $2\sqrt{n_{\text{tot}}n_{\text{imp}}^{\text{hom}}} \rightarrow \frac{1}{2}$. Two regimes may be identified: (1) an *efficient* feedback regime ($g_{\text{fb}} < g_{\text{fb}}^{\text{opt}}$), in which the motion of the oscillator – resulting from the thermal noise and measurement back action – is efficiently suppressed; (2) an *inefficient* feedback regime, in which thermal force and measurement back-action are overwhelmed by *feedback back-action* $n_{\text{fb}} = g_{\text{fb}}^2 n_{\text{imp}}^{\text{hom}}$ (i.e. feedback of homodyne imprecision noise), resulting in an increase of n_m . We explore these regimes in two experiments.

An experimental demonstration of efficient feedback cooling, where feedback back-action is weak ($n_{\text{fb}} < n_{\text{tot}}$), is shown in Fig. 3. Here $n_{\text{tot}} \approx 7 \cdot 10^4$, corresponding to an effective bath temperature of 13 K (arising partly due to quantum measurement back-action, $n_{\text{ba}} \approx 4 \cdot 10^4$ [17]). From the perspective of the heterodyne measurement, the objective is to ‘distill’ a motional sideband asymmetry of one phonon out of n_{tot} . This is made possible by a low shot-noise-limited homodyne imprecision of $n_{\text{imp}}^{\text{hom}} \approx 1.2 \cdot 10^{-4}$ (see Fig. 3d for details). To trace out the cooling curve in Fig. 3a, the feedback gain is tuned electronically while keeping all other experimental parameters (such as mean optical power and laser-cavity detuning) fixed. Sideband ratio R is extracted from fitting a Lorentzian to each heterodyne sideband and taking the ratio of the fitted areas. The phonon occupation n_m is inferred from R as well as the area beneath the lower sideband. In-loop (homodyne) and out-of-loop (heterodyne) noise spectra are shown in Fig. 3b. As a characteristic of the efficient feedback regime, the area under the left sideband decreases linearly with g_{fb} , corresponding to $n_m \propto g_{\text{fb}}^{-1}$ (red circles in Fig. 3a). As the optimal

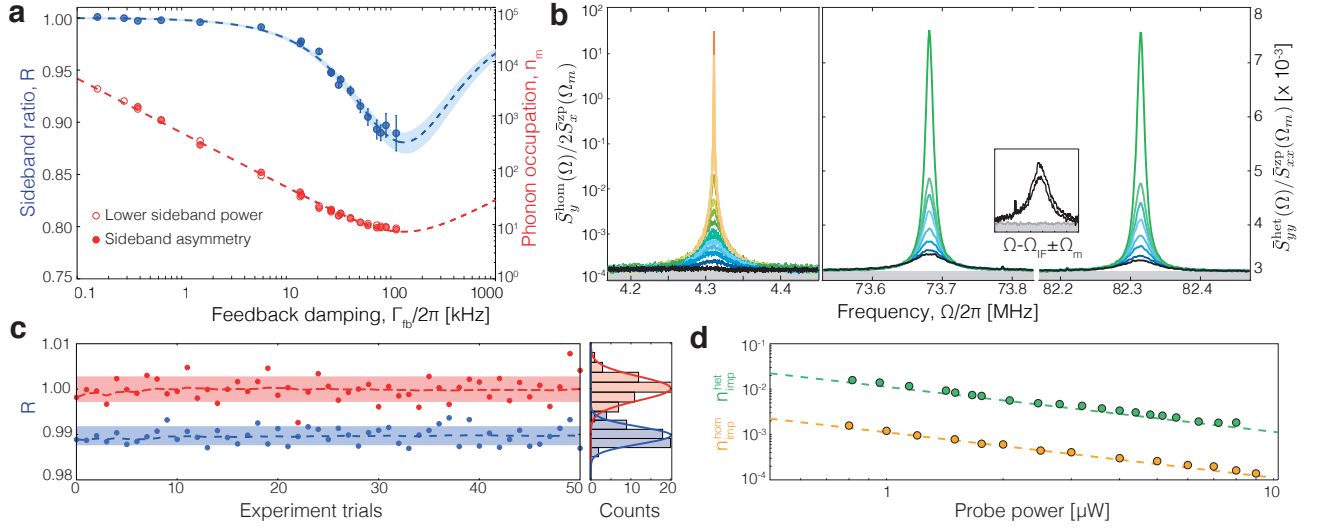


FIG. 3. **Motional sideband asymmetry in the heterodyne measurement of a cold-damped mechanical oscillator.**

(a) Heterodyne sideband asymmetry (R , blue) and inferred mechanical mode occupation (n_m , red) versus closed-loop mechanical damping rate (Γ_{fb}) for various feedback gains. A maximum asymmetry of $1 - R \approx 12\%$ ($n_m \approx 7.3$) appears as the feedback gain approaches its optimal value. Dashed lines correspond to models $R = \frac{n_m}{n_m + 1}$ (Eq. (A25), blue line) and $n_m + \frac{1}{2} \approx \frac{\Gamma_m}{\Gamma_{fb}} n_{tot} + \frac{\Gamma_{fb}}{\Gamma_m} n_{imp}^{hom}$ (Eq. (5), red line). Solid blue band is a confidence interval based on uncertainties in estimates of n_{tot} , n_{imp}^{hom} , and Γ_m . Open red circles are independent estimates of n_m based on the area beneath the left heterodyne sideband. (b) Homodyne (left panel) and heterodyne (right panel) spectra used to obtain (a). Black traces correspond to lowest occupation; asymmetry is highlighted in the inset. Only a subset of heterodyne spectra are shown, for low n_m , with colors matching the corresponding homodyne spectra. An important feature of these spectra are their low imprecision, $n_{imp}^{hom} = (16\eta_{hom}C_0n_c)^{-1} = 1.2 \cdot 10^{-4}$ and $n_{imp}^{het} = (4\eta_{het}C_0n_c)^{-1} = 2.9 \cdot 10^{-3}$. This is made possible by the high photon collection efficiency $\eta \sim 0.2$, single photon cooperativity $C_0 = 4g_0^2/\kappa\Gamma_m = 0.3$, and power handling capacity of the microcavity-based sensor (allowing for intracavity photon numbers of $n_c \sim 10^4$). (c) Statistical fluctuations of R for low feedback gain, indicating the ability to discriminate a 0.5% asymmetry, corresponding to $n_m \approx 100$. (d) Phonon-equivalent imprecision of the heterodyne and homodyne detectors as a function of the power of the meter field.

gain is approached, the in-loop spectrum is reduced to the imprecision noise floor (black trace in Fig. 3b). This transition coincides with the ‘appearance’ of a sideband asymmetry of $1 - R \approx 12\%$ ($\xi \approx 6\%$), corresponding to $n_m \approx 7.3$.

To confirm the faithfulness of these measurements, two major sources of error were investigated:

(1) Drift over the course of measurement can introduce small changes in the relative magnitude of $\bar{S}_{yy}^{het}(\Omega_{het}^\pm)$. In our experiment, this effect is mitigated by recording both heterodyne sidebands simultaneously. Augmented by operating in the bad cavity regime ($\Omega_m/\kappa \sim 10^{-3}$), and the exceptionally low imprecision of the heterodyne measurement, $n_{imp}^{het} = (4\eta_{het}C_0n_c)^{-1} \approx 3 \cdot 10^{-3}$ (see Fig. 3d), statistical fluctuations of R over the course of a typical measurement set can be as small as 0.5% (see Fig. 3c). Error bars for R in Fig. 3a are derived from the standard deviation of similar data sets, in addition to a small contribution from the fit covariance matrix. At the largest damping rates, the reduced heterodyne signal-to-noise results in insufficient convergence of the periodogram estimate of the spectra (keeping acquisition time and analysis bandwidth fixed), leading to larger error bars, $\delta R = \pm 2\%$.

(2) Excess laser noise affects R by producing additional

imprecision-back-action correlations [10, 26]. Assuming a mean thermal photon occupation of $C_{qq(pp)}$ for the amplitude (phase) quadrature of the injected meter field, the correlator in Eq. (1) becomes [22],

$$\frac{2\text{Re} \bar{S}_{x_{ba}x_{imp}}^{het}(\Omega_{het}^\pm)}{\bar{S}_{xx}^{zp}(\Omega_m)} = \mp \eta_{het} \left(\frac{1}{2} + C_{qq} \pm \frac{4\bar{\Delta}\Omega_m}{\kappa^2} C_{pp} \right), \quad (6)$$

where η_{het} is the heterodyne detection efficiency, and $\bar{\Delta}$ is the mean laser-cavity detuning. In our experiment, independent measurements reveal that $C_{qq} < 0.01$ and $C_{pp} < 30$ (owing partly to excess cavity frequency noise) for typical meter powers of $P_{in} < 5 \mu W$ [22]. Operating on resonance ($\bar{\Delta} \approx 0$) and in the bad-cavity regime substantially reduces sensitivity to C_{pp} . Using a typical value of $\bar{\Delta} = 0.01 \cdot \kappa$, we estimate that $\frac{4\bar{\Delta}\Omega_m}{\kappa^2} C_{pp} < 0.005$ negligibly to Eq. (6).

Having established that our measurements of motional sideband asymmetry are not contaminated by classical artefacts, the results shown in Fig. 3 may be interpreted as a ‘distillation’ of quantum correlations using efficient feedback. We now explore the complementary regime of inefficient feedback, where feedback back-action is stronger than the thermal force and measurement back-

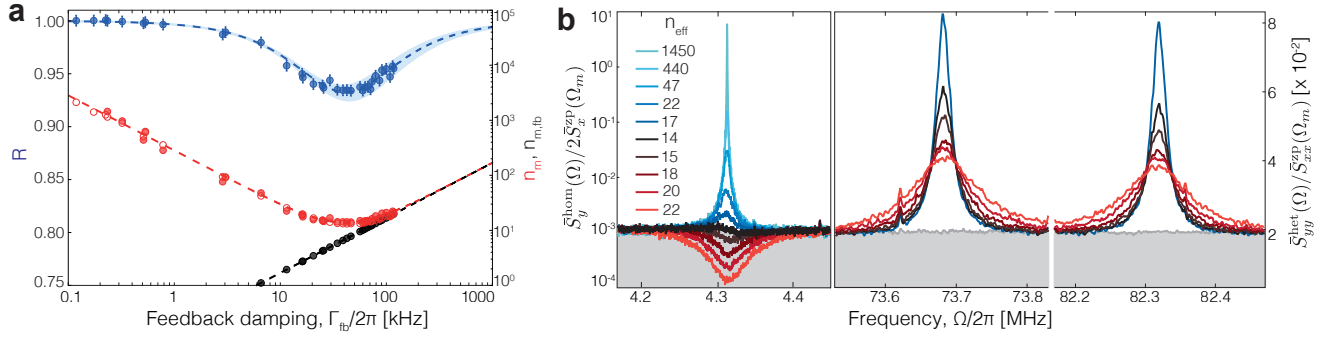


FIG. 4. **Appearance and disappearance of sideband asymmetry.** (a) Repeat of the experiment shown in Fig. 3a with lower homodyne detection efficiency. Feedback with the same range of gain results in lower optimal asymmetry ($R \approx 6\%$) and accesses to a ‘strong feedback’ regime in which feedback back-action (n_{fb}) dominates physical motion, resulting in reduced R . Black points are an estimate of the mechanical occupation due to feedback back-action, $n_{m,fb} = \frac{\Gamma_m}{\Gamma_{fb}} n_{fb} = g_{fb} n_{imp}^{hom}$, based on the noise floor of the homodyne spectra. (b) Left panel: In-loop homodyne spectra. In the strong feedback regime, noise is ‘squashed’ (reduced below the open-loop imprecision), corresponding to in-loop squeezing. Right panel: Out-of-loop heterodyne spectra. Inefficient feedback manifests as an increase in the off-resonant noise power and reduced asymmetry.

action ($n_{fb} > n_{tot}$). We access this regime by changing the homodyne/heterodyne splitting ratio, thereby increasing the homodyne imprecision to $n_{imp}^{hom} \approx 10^{-3}$. As shown in Fig. 4, increasing the gain beyond its optimum value (corresponding to $n_m \approx 13.4$ and $1 - R \approx 7\%$), results in a reduction of the homodyne signal below the shot-noise level (Fig. 4b left panel). Simultaneously, the areas of the heterodyne sidebands increase, while their asymmetry ($1 - R$) decreases. The discrepancy between ‘squashing’ [19, 27] of the in-loop signal and the ‘disappearance’ of sideband asymmetry relates to a basic difference between feedback back-action and meter back-action, namely, feedback back-action is correlated with the in-loop imprecision and not with the out-of-loop imprecision [19].

Squashing of the in-loop signal is caused by correlations between the feedback back-action driven motion x_{fb}

and the in-loop measurement imprecision [22],

$$\frac{2\text{Re}\bar{S}_{x_{fb}x_{imp}}^{hom}(\Omega_m)}{2\bar{S}_{xx}^{zp}(\Omega_m)} = -n_{imp}^{hom}g_{fb}. \quad (7)$$

represented by the negative-valued green trace in Fig. 1b (left panel). Interestingly, these classical correlations, in conjunction with the generalized Heisenberg uncertainty principle [2, 3] can be used to predict the transition from efficient to inefficient feedback; viz.

$$\bar{S}_{FF} \cdot \bar{S}_{xx}^{imp,hom} \geq \frac{\hbar^2}{2} + (2\text{Re}\bar{S}_{Fx_{imp,hom}})^2, \quad (8)$$

is saturated for $g_{fb}^{opt} = \sqrt{n_{tot}/n_{imp}^{hom}}$ (using $F_{fb} \propto g_{fb}x_{imp}^{hom}$ and Eq. (7)). The limits of feedback cooling, and the prospects for feedback-based enhancement of quantum correlations, is related to the detection of meter fluctuations and the choice of feedback strategy – optimization of either seems pertinent.

-
- [1] H. M. Wiseman and G. J. Milburn, *Quantum Measurement and Control* (Cambridge University Press, 2010).
 - [2] V. Braginsky and F. Khalili, *Quantum Measurement* (Cambridge University Press, 1992).
 - [3] A. A. Clerk, M. H. Devoret, S. M. Girvin, F. Marquardt, and R. J. Schoelkopf, *Rev. Mod. Phys.* **82**, 1155 (2010).
 - [4] LIGO Scientific Collaboration and Virgo Collaboration, *Phys. Rev. Lett.* **116**, 131103 (2016).
 - [5] D. W. C. Brooks, T. Botter, S. Schreppler, T. P. Purdy, N. Brahms, and D. M. Stamper-Kurn, *Nature* **488**, 476 (2012).
 - [6] A. H. Safavi-Naeini, S. Gröblacher, J. T. Hill, J. Chan, M. Aspelmeyer, and O. Painter, *Nature* **500**, 185 (2013).
 - [7] T. P. Purdy, P. Yu, R. W. Peterson, N. S. Kampel, and C. A. Regal, *Phys. Rev. X* **3**, 031012 (2013).
 - [8] W. H. P. Nielsen, Y. Tsaturyan, C. B. Moller, E. S. Polzik, and A. Schliesser, [arXiv:1605.06541](https://arxiv.org/abs/1605.06541) (2016).
 - [9] A. H. Safavi-Naeini, J. Chan, J. T. Hill, T. P. M. Alegre, A. Krause, and O. Painter, *Phys. Rev. Lett.* **108**, 033602 (2012).
 - [10] A. Weinstein, C. Lei, E. Wollman, J. Suh, A. Metelmann, A. Clerk, and K. Schwab, *Phys. Rev. X* **4**, 041003 (2014).
 - [11] T. P. Purdy, P.-L. Yu, N. S. Kampel, R. W. Peterson, K. Cicak, R. W. Simmonds, and C. A. Regal, *Phys. Rev. A* **92**, 031802 (2015).
 - [12] M. Underwood, D. Mason, D. Lee, H. Xu, L. Jiang, A. B. Shkarin, K. Børkje, S. M. Girvin, and J. G. E. Harris, *Phys. Rev. A* **92**, 061801 (2015).
 - [13] J. H. Shapiro, *IEEE J. Quant. Elec.* **21**, 237 (1985).
 - [14] F. Khalili, H. Miao, H. Yang, A. Safavi-Naeini,

- O. Painter, and Y. Chen, *Phys. Rev. A* **86**, 033840 (2012).
- [15] L. F. Buchmann, S. Schreppler, J. Kohler, N. Spethmann, and D. M. Stamper-Kurn, *arXiv:1602.02141* (2016).
- [16] Note that sideband asymmetry arising for direct photon counting of the meter field has a different origin [10].
- [17] D. J. Wilson, V. Sudhir, N. Piro, R. Schilling, A. Ghadimi, and T. J. Kippenberg, *Nature* **524**, 325 (2015).
- [18] M. Hatridge, S. Shankar, M. Mirrahimi, F. Shackert, K. Geerlings, T. Brecht, K. Sliwa, B. Abdo, L. Frunzio, S. M. Girvin, R. J. Schoelkopf, and M. H. Devoret, *Science* **339**, 178 (2013).
- [19] M. S. Taubman, H. Wiseman, D. E. McClelland, and H.-A. Bachor, *J. Opt. Soc. Am. B* **12**, 1792 (1995).
- [20] R. W. Peterson, T. P. Purdy, N. S. Kampel, R. W. Andrews, L. K. W. Yu, P.-L., and C. A. Regal, *Phys. Rev. Lett.* **116**, 063601 (2016).
- [21] Here, heterodyne spectra are expressed as double-sided symmetrized spectra, for example \bar{S}_{yy} , while homodyne spectra are expressed as the corresponding single-sided symmetrized versions, for example \bar{S}_y .
- [22] See Supplementary Information.
- [23] R. Schilling, H. Schütz, A. Ghadimi, V. Sudhir, D. Wilson, and T. Kippenberg, *Phys. Rev. Applied* **5**, 054019 (2016).
- [24] C. Fabre, M. Pinard, S. Bourzeix, A. Heidmann, E. Giacobino, and S. Reynaud, *Phys. Rev. A* **49**, 1337 (1994).
- [25] J. Courty, A. Heidmann, and M. Pinard, *Eur. Phys. J. D* **17**, 399 (2001).
- [26] A. M. Jayich, J. C. Sankey, K. Børkje, D. Lee, C. Yang, M. Underwood, L. Childress, A. Petrenko, S. M. Girvin, and J. G. E. Harris, *New J. Phys.* **14**, 115018 (2012).
- [27] H. M. Wiseman, *J. Opt. B* **1**, 459 (1999).
- [28] A. H. Safavi-Naeini, J. Chan, J. T. Hill, S. Gröblacher, H. Miao, Y. Chen, M. Aspelmeyer, and O. Painter, *New J. Phys.* **15**, 035007 (2013).
- [29] In addition, it is known that for semiconductor lasers, phase-amplitude correlations are limited to frequencies close to their relaxation oscillation frequency [39, 40]; the latter is typically at a few GHz from the carrier [41] – irrelevant for our experiment.
- [30] M. Aspelmeyer, T. J. Kippenberg, and F. Marquardt, *Rev. Mod. Phys.* **86**, 1391 (2014).
- [31] C. Gardiner and M. Collett, *Phys. Rev. A* **31**, 3761 (1985).
- [32] M. L. Gorodetsky and I. S. Grudinin, *JOSA B* **21**, 697 (2004).
- [33] A. Gillespie and F. Raab, *Phys. Lett. A* **178**, 357 (1993).
- [34] G. C. Bjorklund, *Opt. Lett.* **5**, 15 (1980).
- [35] M. L. Gorodetsky, A. Schliesser, G. Anetsberger, S. Deleglise, and T. J. Kippenberg, *Opt. Exp.* **18**, 23236 (2010).
- [36] V. B. Braginsky, M. L. Gorodetsky, and S. P. Vyatchanin, *Phys. Lett. A* **271**, 303 (2000).
- [37] H. Cramer, *Mathematical Methods of Statistics* (Princeton University Press).
- [38] R. Simon, N. Mukunda, and B. Dutta, *Phys. Rev. A* **49**, 1567 (1994).
- [39] K. Vahala, C. Harder, and A. Yariv, *Appl. Phys. Lett.* **42**, 211 (1983).
- [40] M. van Exeter, W. Hamel, J. P. Woerdman, and B. Zekelman, *IEEE J. Quantum Electronics* **28**, 1470 (1992).
- [41] T. J. Kippenberg, A. Schliesser, and M. L. Gorodetsky, *New J. Phys.* **15**, 015019 (2013).

Appendix A: Excess laser noise

The effect of laser noise on sideband asymmetry measurements is well-studied for cavity optomechanical systems in the resolved sideband regime [26, 28]. In this case sidebands have been observed separately by scattering them into the cavity with a probe laser red/blue detuned. Here we discuss the effect of laser noise on sideband asymmetry measurements in the “bad-cavity” regime ($\Omega_m \ll \kappa$), wherein a resonant probe is used to detect the sidebands simultaneously in a heterodyne measurement. A theoretical model is developed in Sec. A 1. In Sec. A 2, we present measurements confirming the negligible contribution of laser noise to the reported results.

1. Contribution of excess noise for resonant probing and simultaneous detection of sidebands

In our experiment, we probe the optomechanical system using a resonant laser at frequency ω_L . The photon flux amplitude operator of the laser, $a_{\text{in}}(t)$, is assumed to have the form,

$$a_{\text{in}}(t) = e^{-i\omega_L t}(\bar{a}_{\text{in}} + \delta a_{\text{in}}(t)), \quad (\text{A1})$$

where $\bar{a}_{\text{in}} = \sqrt{P_{\text{in}}/\hbar\omega_L}$ is the mean photon flux and the fluctuations $\delta a_{\text{in}}(t)$ satisfy,

$$[\delta a_{\text{in}}(t), \delta a_{\text{in}}^\dagger(t')] = \alpha \delta(t - t'). \quad (\text{A2})$$

Note that we explicitly “tag” the commutator so as to follow its contribution to the measured quantities [10]; in reality $\alpha = 1$.

The canonically conjugate quadratures corresponding to the fluctuations are defined as

$$\begin{aligned} \delta q_{\text{in}}(t) &:= \frac{\delta a_{\text{in}}(t) + \delta a_{\text{in}}^\dagger(t)}{\sqrt{2}}, \\ \delta p_{\text{in}}(t) &:= \frac{\delta a_{\text{in}}(t) - \delta a_{\text{in}}^\dagger(t)}{i\sqrt{2}}, \end{aligned} \quad (\text{A3})$$

so that

$$[\delta q_{\text{in}}(t), \delta p_{\text{in}}(t')] = i\alpha \delta(t - t'). \quad (\text{A4})$$

Excess (“classical”) noise in the laser is modeled as Gaussian fluctuations, for which,

$$\begin{aligned} &\begin{pmatrix} \langle \delta q_{\text{in}}(t) \delta q_{\text{in}}(t') \rangle & \langle \delta q_{\text{in}}(t) \delta p_{\text{in}}(t') \rangle \\ \langle \delta p_{\text{in}}(t) \delta q_{\text{in}}(t') \rangle & \langle \delta p_{\text{in}}(t) \delta p_{\text{in}}(t') \rangle \end{pmatrix} \\ &= \frac{1}{2} \begin{pmatrix} \alpha + 2C_{qq} & i\alpha + 2C_{qp} \\ -i\alpha + 2C_{qp} & \alpha + 2C_{pp} \end{pmatrix} \delta(t - t'). \end{aligned} \quad (\text{A5})$$

The terms C_{ij} ($i = q, p$) represent the noise in excess of the fundamental vacuum fluctuations in the field quadratures, distributed uniformly (i.e. “white”) in frequency. We henceforth omit the cross-correlation C_{qp} and attempt to bound its effect via an appropriate inequality [29] (see Sec. A3). Thus,

$$\begin{aligned} & \begin{pmatrix} \langle \delta a_{\text{in}}(t) \delta a_{\text{in}}(t') \rangle & \langle \delta a_{\text{in}}(t) \delta a_{\text{in}}^\dagger(t') \rangle \\ \langle \delta a_{\text{in}}^\dagger(t) \delta a_{\text{in}}(t') \rangle & \langle \delta a_{\text{in}}^\dagger(t) \delta a_{\text{in}}^\dagger(t') \rangle \end{pmatrix} \\ &= \frac{1}{2} \begin{pmatrix} C_{qq} - C_{pp} & 2\alpha + C_{qq} + C_{pp} \\ C_{qq} + C_{pp} & C_{qq} - C_{pp} \end{pmatrix}. \end{aligned} \quad (\text{A6})$$

We now consider an optomechanical system where the optical cavity is driven by a noisy input field satisfying Eq. (A6). The mechanical oscillator couples to the cavity field via radiation pressure and is additionally driven by a thermal Langevin force. Fluctuations of the intracavity field amplitude (δa) and the mechanical oscillator amplitude (δb) around their stable steady states satisfy

[30]

$$\dot{\delta a} = +i\Delta \delta a - \frac{\kappa}{2} \delta a + ig(\delta b + \delta b^\dagger) + \sqrt{\kappa} \delta a_{\text{in}} \quad (\text{A7})$$

$$\dot{\delta b} = -i\Omega_m \delta b - \frac{\Gamma_m}{2} \delta b + i(g^* \delta a + g \delta a^\dagger) + \sqrt{\Gamma_m} \delta b_{\text{in}} \quad (\text{A8})$$

Here $\Delta = \omega_L - \omega_c$ is the laser detuning, $g = g_0 \bar{a}$ is the dressed (“multi-photon”) optomechanical coupling rate, and $\bar{a} = \frac{\sqrt{\kappa} \bar{a}_{\text{in}}}{\frac{\kappa}{2} - i\Delta}$ is the mean intracavity field amplitude. We have also assumed here that the cavity decay rate is dominated by its external coupling, i.e. $\kappa = \kappa_0 + \kappa_{\text{ex}} \approx \kappa_{\text{ex}}$. The mechanical Langevin noise correlators are

$$\langle \delta b_{\text{in}}(t) \delta b_{\text{in}}^\dagger(t') \rangle = (n_{\text{th}} + \beta) \delta(t - t') \quad (\text{A9})$$

$$\langle \delta b_{\text{in}}^\dagger(t) \delta b_{\text{in}}(t') \rangle = n_{\text{th}} \delta(t - t'), \quad (\text{A10})$$

where n_{th} is the ambient mean thermal phonon occupation of the oscillator. Note that we also “tag” the contribution due to the zero-point fluctuation of the thermal bath to determine its role in the observables; in reality $\beta = 1$.

Equations (A7) and (A8) can be solved in the Fourier domain,

$$\delta a[\Omega] = \chi_c[\Omega] [\sqrt{\kappa} \delta a_{\text{in}}[\Omega] + ig(\delta b[\Omega] + \delta b^\dagger[\Omega])] \quad (\text{A11})$$

$$\delta a^\dagger[\Omega] = \delta a[-\Omega]^\dagger = \chi_c^*[-\Omega] [\sqrt{\kappa} \delta a_{\text{in}}^\dagger[\Omega] - ig^*(\delta b[\Omega] + \delta b^\dagger[\Omega])] \quad (\text{A12})$$

$$\begin{aligned} \begin{pmatrix} \delta b[\Omega] \\ \delta b^\dagger[\Omega] \end{pmatrix} &= \frac{\sqrt{\Gamma_m}}{\mathcal{N}[\Omega]} \begin{pmatrix} \chi_m^{*-1}[-\Omega] - i\Sigma[\Omega] & -i\Sigma[\Omega] \\ +i\Sigma[\Omega] & \chi_m^{-1}[\Omega] + i\Sigma[\Omega] \end{pmatrix} \begin{pmatrix} \delta b_{\text{in}}[\Omega] \\ \delta b_{\text{in}}^\dagger[\Omega] \end{pmatrix} \\ &+ \frac{i\sqrt{\kappa}}{\mathcal{N}[\Omega]} \begin{pmatrix} g^* \chi_m^{*-1}[-\Omega] \chi_c[\Omega] & g \chi_m^{*-1}[-\Omega] \chi_c^*[-\Omega] \\ -g^* \chi_m^{-1}[\Omega] \chi_c[\Omega] & -g \chi_m^{-1}[\Omega] \chi_c^*[-\Omega] \end{pmatrix} \begin{pmatrix} \delta a_{\text{in}}[\Omega] \\ \delta a_{\text{in}}^\dagger[\Omega] \end{pmatrix}. \end{aligned}$$

Here χ_m and χ_c are the bare mechanical and cavity response functions, respectively, given by,

$$\begin{aligned} \chi_m[\Omega] &:= [\Gamma_m/2 - i(\Omega - \Omega_m)]^{-1}, \\ \chi_c[\Omega] &:= [\kappa/2 - i(\Omega + \Delta)]^{-1}. \end{aligned} \quad (\text{A13})$$

$\Sigma[\Omega]$ is the mechanical “self-energy”,

$$\Sigma[\Omega] = -i|g|^2(\chi_c[\Omega] - \chi_c^*[-\Omega]) = \Sigma^*[-\Omega], \quad (\text{A14})$$

which describes the modification to the mechanical response due to radiation pressure, and

$$\mathcal{N}[\Omega] = \chi_m^{-1}[\Omega] \chi_m^{*-1}[-\Omega] + 2\Omega_m \Sigma[\Omega] = \mathcal{N}^*[-\Omega]. \quad (\text{A15})$$

The input-output relation [31], $\delta a_{\text{out}} = \delta a_{\text{in}} - \sqrt{\kappa} \delta a$, gives the fluctuations of the output fields in terms of the fluctuations of the input fields:

$$\delta a_{\text{out}} = A[\Omega] \delta a_{\text{in}} + B[\Omega] \delta a_{\text{in}}^\dagger + C[\Omega] \delta b_{\text{in}} + D[\Omega] \delta b_{\text{in}}^\dagger \quad (\text{A16})$$

where,

$$\begin{aligned}
A[\Omega] &= 1 - \kappa\chi_c[\Omega] - \frac{2i|g|^2\kappa\Omega_m\chi_c[\Omega]^2}{\mathcal{N}[\Omega]} \approx -\left(1 + 4i\frac{\Delta}{\kappa}\right)\left(1 + C_0n_c\frac{2i\Omega_m\Gamma_m}{\mathcal{N}[\Omega]}\right) \\
B[\Omega] &= -\frac{2ig^2\kappa\Omega_m\chi_c[\Omega]\chi_c^*[-\Omega]}{\mathcal{N}[\Omega]} \approx -C_0n_c\frac{2i\Omega_m\Gamma_m}{\mathcal{N}[\Omega]} \\
C[\Omega] &= -\frac{ig\sqrt{\kappa\Gamma_m}}{\mathcal{N}[\Omega]}\chi_c[\Omega]\chi_m^{*-1}[-\Omega] \approx -i\sqrt{C_0n_c}\left(1 + 2i\frac{\Delta}{\kappa}\right)\Gamma_m\chi_m[\Omega] \\
D[\Omega] &= -\frac{ig\sqrt{\kappa\Gamma_m}}{\mathcal{N}[\Omega]}\chi_c[\Omega]\chi_m^{-1}[\Omega] \approx -i\sqrt{C_0n_c}\left(1 + 2i\frac{\Delta}{\kappa}\right)\Gamma_m\chi_m^*[-\Omega].
\end{aligned} \tag{A17}$$

Here approximate expressions are given for the case of interest, namely, resonant probing ($|\Delta| \ll \kappa$), small sideband resolution ($\Omega_m \ll \kappa$), and weak coupling ($|g| \ll \kappa$). We have also introduced the single-photon cooperativity, $C_0 = 4g_0^2/(\kappa\Gamma_m)$, and the mean intracavity photon number, $n_c = |\bar{a}|^2$.

Balanced heterodyne detection of the cavity output is used to measure motional sideband asymmetry. The output field is superposed on a balanced beamsplitter with a frequency-shifted local oscillator,

$$a_{\text{LO}} = e^{-i(\omega_L + \Omega_{\text{IF}})t}(\bar{a}_{\text{LO}} + \delta a_{\text{LO}}). \tag{A18}$$

The fields at the output of the beamsplitter, $\frac{1}{\sqrt{2}}(a_{\text{LO}} \pm a_{\text{out}})$, are detected with identical square-law detectors, whose photocurrents are subtracted. Note the implicit assumption that the local oscillator and signal paths are balanced in length; together with a balance of power beyond the combining beamsplitter, this ensures suppression of common-mode excess noise [13].

The difference photocurrent is described by the operator,

$$I \propto a_{\text{LO}}^\dagger a_{\text{out}} + \text{H.c.} \tag{A19}$$

When $\bar{a}_{\text{LO}} \gg \bar{a}_{\text{out}}$, fluctuations in the photocurrent are described by

$$\delta I(t) \propto e^{-i\Omega_{\text{IF}}t} \bar{a}_{\text{LO}}^* \delta a_{\text{out}}(t) + \text{H.c.} \tag{A20}$$

The power spectrum of the heterodyne photocurrent is proportional to

$$\bar{S}_{II}^{\text{het}}(\Omega) = \frac{1}{2} \int_{-\infty}^{\infty} \langle \overline{\{\delta I(t+t'), \delta I(t')\}} \rangle e^{i\Omega t} dt, \tag{A21}$$

where we have introduced the (time-averaged) current correlator,

$$\begin{aligned}
\overline{\{\delta I(t+t'), \delta I(t')\}} &\propto e^{-i\Omega_{\text{IF}}t} \left\{ \delta a_{\text{out}}^\dagger(t), \delta a_{\text{out}}(0) \right\} \\
&\quad + e^{+i\Omega_{\text{IF}}t} \left\{ \delta a_{\text{out}}(t), \delta a_{\text{out}}^\dagger(0) \right\}.
\end{aligned} \tag{A22}$$

Assuming $\Omega_{\text{IF}} \gg \Omega_m > 0$, we obtain for the balanced heterodyne spectrum normalized to the local oscillator shot noise,

$$\begin{aligned}
\bar{S}_{II}^{\text{het}}(\Omega - \Omega_{\text{IF}}) &\approx \alpha + 4C_0n_c \left[\frac{\Gamma_m^2}{4} |\chi_m[-\Omega]|^2 \left(n_{\text{tot}} + \frac{\beta}{2} - \left(\frac{\alpha}{2} + C_{qq} \right) + \frac{4\Delta\Omega_m}{\kappa^2} C_{pp} \right) \right. \\
&\quad \left. + \frac{\Gamma_m^2}{4} |\chi_m[\Omega]|^2 \left(n_{\text{tot}} + \frac{\beta}{2} + \left(\frac{\alpha}{2} + C_{qq} \right) + \frac{4\Delta\Omega_m}{\kappa^2} C_{pp} \right) \right].
\end{aligned} \tag{A23}$$

This represents the heterodyne spectrum measured in the experiment and depicted in Fig.2 and Fig.3 of the main text. Here the total bath occupation, arising from the ambient thermal bath and the measurement back-action due to the meter beam, is given by,

$$n_{\text{tot}} = n_{\text{th}} + \underbrace{C_0n_c \left(\frac{\alpha}{2} + C_{qq} + \left(\frac{4\Delta\Omega_m}{\kappa^2} \right)^2 C_{pp} \right)}_{n_{\text{ba}}}. \tag{A24}$$

The *sideband ratio* extracted from such a spectrum is,

$$\begin{aligned}
R &:= \frac{\int_{0+}^{+\infty} (\bar{S}_{II}^{\text{het}}(\Omega - \Omega_{\text{IF}}) - \bar{S}_{II}^{\text{het}}(\Omega = \Omega_{\text{IF}}^+)) \frac{d\Omega}{2\pi}}{\int_{-\infty}^{0-} (\bar{S}_{II}^{\text{het}}(\Omega - \Omega_{\text{IF}}) - \bar{S}_{II}^{\text{het}}(\Omega = \Omega_{\text{IF}}^-)) \frac{d\Omega}{2\pi}} \\
&= \frac{n_{\text{tot}} + \frac{\beta - \alpha}{2} - C_{qq} + \frac{4\Delta\Omega_m}{\kappa^2} C_{pp}}{n_{\text{tot}} + \frac{\beta + \alpha}{2} + C_{qq} + \frac{4\Delta\Omega_m}{\kappa^2} C_{pp}} \\
&= \frac{n_{\text{tot}} + \left(\frac{4\Delta\Omega_m}{\kappa^2} C_{pp} - C_{qq} \right)}{n_{\text{tot}} + 1 + \left(\frac{4\Delta\Omega_m}{\kappa^2} C_{pp} + C_{qq} \right)}.
\end{aligned} \tag{A25}$$

Firstly, characteristic of linear detection, deviation of R from unity in the ideal case ($C_{qq} = 0 = C_{pp}$) is due

to correlations developed between the quantum-back-action driven mechanical motion and the detection process [10, 28]. When C_{qq} and C_{pp} are finite, classical correlations are established that affect R . The response of the cavity (for $\Delta/\kappa \approx 0$) ensures that excess classical correlations due to input amplitude noise lead to an enhanced asymmetry, whereas those arising from input phase noise lead to a common increase in the sideband noise power.

a. Expression for $\bar{S}_{yy}^{\text{het}}(\Omega)$

In order to compare with Eq.(1) of the main text, we identify the heterodyne spectrum Eq. (A23) with that of a position-equivalent heterodyne observable y_{het} , viz.,

$$\begin{aligned} \bar{S}_{yy}^{\text{het}}(\Omega - \Omega_{\text{IF}}) = & \underbrace{\left(\frac{1}{4C_0 n_c} \right) \bar{S}_{xx}^{\text{zp}}(\Omega_m)}_{\bar{S}_{xx}^{\text{imp,het}}(\Omega)} \\ & + \underbrace{\frac{\Gamma_m^2}{4} \left(|\chi_m[-\Omega]|^2 + |\chi_m[\Omega]|^2 \right) \left(n_{\text{tot}} + \frac{1}{2} \right) \bar{S}_{xx}^{\text{zp}}(\Omega_m)}_{\bar{S}_{xx}^{\text{tot}}(\Omega)} \\ & + \underbrace{\frac{\Gamma_m^2}{4} \left(|\chi_m[-\Omega]|^2 \left(\frac{1}{2} + C_{qq} + \frac{4\Delta\Omega_m}{\kappa^2} C_{pp} \right) + |\chi_m[\Omega]|^2 \left(-\frac{1}{2} - C_{qq} + \frac{4\Delta\Omega_m}{\kappa^2} C_{pp} \right) \right)}_{2\text{Re } \bar{S}_{x\text{ba}x\text{imp}}^{\text{het}}(\Omega)}. \end{aligned} \quad (\text{A26})$$

The identification is made by comparing the magnitude of the total thermal noise signal $\bar{S}_{xx}^{\text{tot}}$.

b. Sensitivity of heterodyne and homodyne readout

In the main text, frequent use is made of the phonon-equivalent sensitivity of the heterodyne and homodyne detectors. The sensitivity of balanced heterodyne detection (for the ideal case $\eta_{\text{het}} = 1$), quantified as imprecision quanta,

$$n_{\text{imp}}^{\text{het}} = (4\eta_{\text{het}} C_0 n_c)^{-1} \quad (\text{A27})$$

is reduced by a factor of 4 compared to balanced homodyne detection (for the ideal case $\eta_{\text{hom}} = 1$) of the phase quadrature of the output field, for which

$$n_{\text{imp}}^{\text{hom}} = (16\eta_{\text{hom}} C_0 n_c)^{-1}. \quad (\text{A28})$$

This loss arises in equal part due to (a) the fact that the heterodyne spectrum is double-sided, and, (b) the detection of both quadratures of the output field.

2. Measurement of excess laser noise

a. Excess amplitude noise

In order to measure the noise in the amplitude quadrature, we employ direct photodetection of the probe laser. The measurement is made at the output of the tapered fiber, with the fiber retracted from the cavity. Analysis of the resulting photocurrent reveals the single-sided

spectrum of the incident optical intensity (referred here for convenience to the incident optical power $P = \hbar\omega_L \dot{n}$),

$$\bar{S}_P(\Omega) = (\hbar\omega_L)^2 \cdot 2\bar{S}_{\dot{n}\dot{n}}(\Omega) = (\hbar\omega_L)^2 \cdot 2\langle \dot{n} \rangle (1 + 2C_{qq}). \quad (\text{A29})$$

A convenient characterization of the intensity noise is via the relative intensity noise (RIN) spectrum,

$$\bar{S}_{\text{RIN}}(\Omega) := \frac{\bar{S}_P(\Omega)}{\langle P \rangle^2} \quad (\text{A30})$$

excess amplitude noise manifests as a deviation from the shot-noise scaling $\propto \frac{1}{\langle P \rangle}$; more precisely,

$$C_{qq} = \frac{1}{2} \left(\frac{\langle \dot{n} \rangle}{2} \bar{S}_{\text{RIN}}(\Omega) - 1 \right). \quad (\text{A31})$$

Fig. 5 shows an inference of C_{qq} using Eq. (A31) and a measurement of $\bar{S}_{\text{RIN}}(\Omega)$ versus mean optical power. For typical experimental conditions ($\langle P \rangle = 1-5 \mu\text{W}$), $C_{qq} \ll 0.01$, so that its contribution to sideband asymmetry is negligible.

b. Excess phase noise

Noise in the phase quadrature of the field leaking from the cavity is measured using balanced homodyne detection. This signal reveals phase noise originating from the input laser as well as apparent phase noise from the cavity. Referred to cavity frequency noise, the homodyne photocurrent spectral density is given by,

$$\begin{aligned} \bar{S}_\omega(\Omega) = \Omega^2 \bar{S}_\phi(\Omega) = \Omega^2 \left(\bar{S}_\phi^{\text{in,shot}}(\Omega) + \bar{S}_\phi^{\text{in,ex}}(\Omega) \right. \\ \left. + \bar{S}_\phi^{\text{cav,ex}}(\Omega) + \bar{S}_\phi^{\text{cav,mech}}(\Omega) \right). \end{aligned} \quad (\text{A32})$$

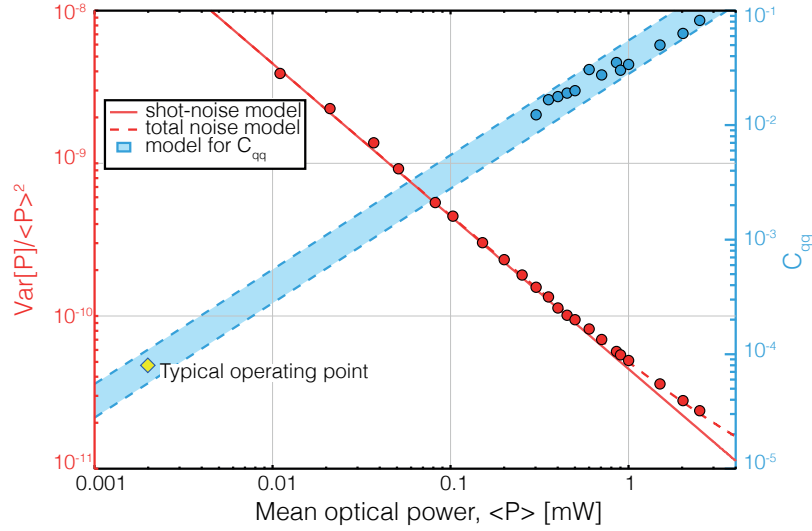


FIG. 5. Integrated (in a 100 kHz band) relative intensity noise $\frac{\text{Var}[P]}{\langle P \rangle^2} := \int \bar{S}_{\text{RIN}}(\Omega \approx \Omega_m) \frac{d\Omega}{2\pi}$ versus mean optical power. Deviation from shot-noise scaling is evident for $\langle P \rangle \gtrsim 1$ mW, attributed to classical amplitude noise.

\bar{S}_ω contains contributions from laser phase noise (shot and excess), cavity substrate noise (including thermorefractive [32] and thermomechanical noise [33]) and thermal motion of other modes of the mechanical resonator. The total excess noise in the phase quadrature is modeled by C_{pp} , which allows us to infer the latter using,

$$\frac{C_{pp}}{\langle \dot{n} \rangle} = \bar{S}_\phi^{\text{in,ex}}(\Omega_m) + \bar{S}_\phi^{\text{cav,ex}}(\Omega_m). \quad (\text{A33})$$

Fig. 6c shows a homodyne measurement made with 3 mW of local oscillator power, whose shot-noise has been subtracted. The spectrum is calibrated by referencing it against a known phase modulation tone injected at the input of the homodyne interferometer [35]. The total excess frequency noise (red) is dominated by thermal motion of the in-plane and out-of-plane modes, both of which are gas damped for this measurement. A joint fit to (a) a model of a velocity-damped oscillator (blue, dashed) and, (b) a model combining thermorefractive [32, 36] and white frequency noise (black, dashed), gives an estimate of $\bar{S}_\omega^{\text{ex}}(\Omega)$. Frequency noise intrinsic to the diode laser was independently measured using an imbalanced interferometer, consistent with the model used to fit the total observed frequency noise. Near the mechanical frequency, $\bar{S}_\omega^{\text{ex}}(\Omega_m) \approx 2\pi \cdot (35 \text{ Hz}/\sqrt{\text{Hz}})^2$, implying (via Eq. (A33)), $C_{pp} \approx 30$ (using signal power of ≈ 100 nW).

From this estimate of C_{pp} we are able to bound two quantities. First, in conjunction with $C_{qq} \ll 0.01$, the excess noise cross-correlation is bounded as $C_{qp} \ll 1$. Secondly, referring to Eq. (A23), we are able to estimate the contribution of phase noise to the heterodyne sideband. This contribution, characterized as an equivalent phonon occupation (since it adds positive noise power to

either sideband),

$$n_\phi = \frac{\Delta}{\kappa} \frac{4\Omega_m}{\kappa} C_{pp}, \quad (\text{A34})$$

has a mean value determined by the mean offset in the detuning $\bar{\Delta}$. Fig. 6a allows an estimate, $\bar{\Delta} \approx 0.01 \cdot \kappa$, giving,

$$\begin{aligned} \bar{n}_\phi &= \frac{\bar{\Delta}}{\kappa} \frac{4\Omega_m}{\kappa} C_{pp} \\ &= 0.0052 \cdot \left(\frac{\bar{\Delta}/\kappa}{0.01} \right)^4 \left(\frac{\Omega_m/2\pi}{4.3 \text{ MHz}} \right) \left(\frac{1 \text{ GHz}}{\kappa/2\pi} \right) \left(\frac{C_{pp}}{30} \right). \end{aligned} \quad (\text{A35})$$

Low frequency detuning noise $\delta\Delta$ (Fig. 6b) causes deviations from this mean, which are significant if their effect is comparable to \bar{n}_ϕ . We bound the probability for such “large” statistical excursions using Chebyshev’s inequality [37],

$$\begin{aligned} \Pr(|n_\phi - \bar{n}_\phi| > \bar{n}_\phi) &\leq \frac{\text{Var}[n_\phi]}{\bar{n}_\phi^2} \\ &= \left(\frac{4\Omega_m}{\kappa} \frac{C_{pp}}{\bar{n}_\phi} \right)^2 \frac{\text{Var}[\delta\Delta]}{\kappa^2} \\ &\approx 10^{-6}. \end{aligned} \quad (\text{A36})$$

We thus estimate that mean residual detuning is the leading contribution to phase noise contamination; the contamination, characterized as a phonon-equivalent noise power $\bar{n}_\phi = 0.005$ is however an insignificant contribution to the sideband ratio Eq. (A25).

Together with the bounds, $C_{qq} \ll 0.01$ and $C_{qp} \ll 1$, this implies that sources of classical noise may be excluded in the interpretation of the experimental data.

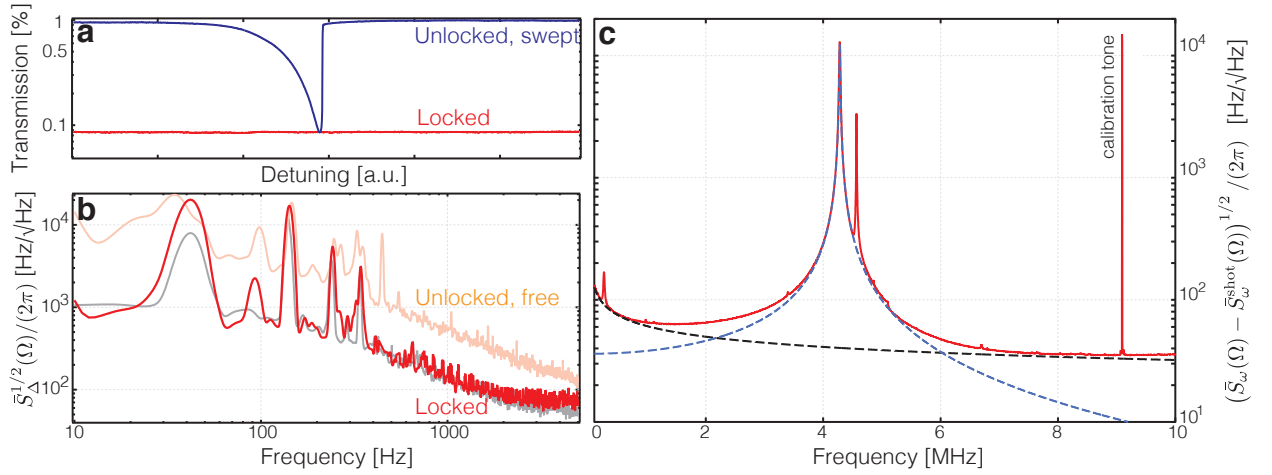


FIG. 6. (a) Residual detuning offset at DC estimated from transmission signal when the laser is locked to cavity. (b) Spectrum analysis of the lock error signal, generated via frequency-modulation spectroscopy [34], reveals low frequency detuning jitter; when locked (red), apparent detuning noise is limited by electronic noise (gray) in the feedback loop, predominantly from the photodetector. (c) Excess frequency noise around the mechanical frequency inferred from a balanced homodyne measurement of the cavity output on resonance. The shot-noise-subtracted signal (red) is composed of the thermomechanical motion of the mechanical mode (blue dashed) and a contribution from excess frequency noise in the laser and cavity substrate (black dashed).

3. Bounding the value of the classical noise cross-correlation C_{qp}

In [26], excess classical noise in the laser is modelled as an independent classical stochastic process introduced explicitly into δa_{in} . The added term, being a classical stochastic process, obeys a Cauchy-Schwarz inequality for its second moments, resulting in the inequality $C_{qp} \leq \sqrt{C_{qq}C_{pp}}$, which may be employed to bound the magnitude of C_{qp} , given measurements of C_{qq} and C_{pp} .

Here we consider a more natural alternative, where the ansatz Eq. (A6) is supposed to arise from a choice of the underlying quantum state that models the classical component of the noise. From this perspective, the ansatz in Eq. (A6) is a valid one as long as it arises from a legitimate quantum state ρ . The sufficient condition for the matrix in Eq. (A6) to be a valid covariance matrix is [38],

$$V := \begin{pmatrix} \frac{1}{2} + C_{qq} & C_{qp} \\ C_{qp} & \frac{1}{2} + C_{pp} \end{pmatrix} \geq 0. \quad (\text{A37})$$

In particular, this implies that $\text{Tr } V \geq 0$ and $\det V \geq 0$; the latter condition gives,

$$\begin{aligned} C_{qp}^2 &\leq C_{qq}C_{pp} + \frac{1}{2}(C_{qq} + C_{pp}) \\ &\leq C_{qq}C_{pp} + \sqrt{C_{qq}C_{pp}} \\ &= C_{qq}C_{pp} \left(1 + \frac{1}{\sqrt{C_{qq}C_{pp}}} \right). \end{aligned} \quad (\text{A38})$$

Here, the second line is obtained by employing the inequality $C_{qq} + C_{pp} \geq 2\sqrt{C_{qq}C_{pp}}$ that follows generally from the fact that $C_{qq,pp}$ are positive.

Ultimately, in the limit $C_{qq}C_{pp} \gg 1$, we recover the result in [26], namely, $C_{qp} \leq (C_{qq}C_{pp})^{1/2}$; however, in

the opposite limit, $C_{qq}C_{pp} \ll 1$, the appropriate bound is $C_{qp} \leq (C_{qq}C_{pp})^{1/4}$, and so employing the conventional Cauchy-Schwarz inequality would lead to an under estimate of C_{qp} .

In our case, $C_{qq}C_{pp} \ll 0.3$, and Eq. (A38) suggests $C_{qp} \ll 1$.

Appendix B: Squeezing in homodyne detection

In the experimentally relevant bad-cavity regime, $\Omega_m \ll \kappa$, resonant probing $\Delta = 0$, and quantum-noise limited probe laser, a significantly simplified analysis illustrates the presence of correlations in the transmitted field.

Following from Eq. (A16) and Eq. (A17), the cavity transmission is given by,

$$\delta a_{\text{out}}[\Omega] \approx -\delta a_{\text{in}}[\Omega] - i \frac{\sqrt{C_0 n_c \Gamma_m}}{x_{zp}} (x_{\text{th}}[\Omega] + x_{\text{ba}}[\Omega]), \quad (\text{B1})$$

where the total motion, $x := x_{zp}(b + b^\dagger)$, has been partitioned into the (intrinsic) thermal motion x_{th} due to the ambient environment,

$$\delta x_{\text{th}}[\Omega] := x_{zp} \sqrt{\Gamma_m} \left(\chi_m[\Omega] \delta b_{\text{in}}[\Omega] + \chi_m[-\Omega]^* \delta b_{\text{in}}^\dagger[\Omega] \right) \quad (\text{B2})$$

and x_{ba} , the back-action driven motion,

$$\begin{aligned} \delta x_{\text{ba}}[\Omega] &:= x_{zp} \sqrt{2C_0 n_c \Gamma_m} \frac{2\Omega_m}{\mathcal{N}[\Omega]} \delta q_{\text{in}}[\Omega] \\ &\approx x_{zp} \sqrt{2C_0 n_c \Gamma_m} \frac{\delta q_{\text{in}}[\Omega]}{(\Omega - \Omega_m) - i(\Gamma_m/2)} \end{aligned} \quad (\text{B3})$$

due to the vacuum fluctuations in the amplitude quadrature of the input optical field. Note that the second equality neglects dynamical back-action and assumes a

high-Q mechanical oscillator.

In terms of the amplitude (δq) and phase (δp) quadratures, Eq. (B1) takes the form,

$$\begin{aligned}\delta q_{\text{out}}[\Omega] &= -\delta q_{\text{in}}[\Omega] \\ \delta p_{\text{out}}[\Omega] &= -\delta p_{\text{in}}[\Omega] - \frac{\sqrt{2C_0 n_c \Gamma_m}}{x_{\text{zp}}} (x_{\text{th}}[\Omega] + x_{\text{ba}}[\Omega]) \\ &= -\delta p_{\text{in}}[\Omega] - \sqrt{2C_0 n_c \Gamma_m} \frac{x_{\text{th}}[\Omega]}{x_{\text{zp}}} - \frac{2C_0 n_c \Gamma_m}{(\Omega - \Omega_m) - i(\Gamma_m/2)} \delta q_{\text{in}}[\Omega].\end{aligned}\quad (\text{B4})$$

Note that the transmitted phase quadrature has a component proportional to the transmitted amplitude quadrature, leading to phase-amplitude correlations described by the (un-symmetrized, double-sided) cross-correlation spectrum,

$$S_{pq}^{\text{out}}(\Omega) = -\frac{i}{2} + \frac{C_0 n_c \Gamma_m}{(\Omega - \Omega_m) - i(\Gamma_m/2)}. \quad (\text{B5})$$

where the first term is due to the commutation relation of the transmitted fields, while the second arises from correlations induced by the optomechanical interaction.

Homodyne detection of the phase quadrature, corresponding to a measurement of δp_{out} alone, does not give access to these optomechanically induced correlations. However, homodyne detection at a finite phase offset θ ,

corresponding to a measurement of,

$$\delta q_{\text{out}}^\theta[\Omega] := \delta q_{\text{out}}[\Omega] \cos \theta + \delta p_{\text{out}}[\Omega] \sin \theta, \quad (\text{B6})$$

can directly access amplitude-phase correlations. Indeed, the homodyne photocurrent spectrum, $\bar{S}_{II}^{\text{hom},\theta}(\Omega) \propto \bar{S}_{qq}^{\text{out},\theta}(\Omega)$, takes the form,

$$\begin{aligned}\bar{S}_{II}^{\text{hom},\theta}(\Omega) &\propto \cos^2 \theta \bar{S}_{qq}^{\text{out}}(\Omega) + \sin^2 \theta \bar{S}_{pp}^{\text{out}}(\Omega) \\ &\quad + \sin(2\theta) \text{Re } S_{pq}^{\text{out}}(\Omega),\end{aligned}\quad (\text{B7})$$

so that for $\theta \neq 0, \pi/2$, the correlation term is manifest. Including the effect of non-ideal detection efficiency, $\eta_{\text{hom}} \leq 1$, and normalizing to shot-noise, the homodyne photocurrent spectrum is,

$$\bar{S}_{II}^{\text{hom},\theta}(\Omega) = 1 + 4C_0 n_c \eta_{\text{hom}} \frac{\bar{S}_{xx}(\Omega)}{x_{\text{zp}}^2} \sin^2 \theta + \underbrace{2C_0 n_c \eta_{\text{hom}} \frac{\Gamma_m(\Omega - \Omega_m)}{(\Omega - \Omega_m)^2 + (\Gamma_m/2)^2} \sin(2\theta)}_{2\text{Re } \bar{S}_{x_{\text{ba}} x_{\text{imp}}}^{\text{hom},\theta}(\Omega)}. \quad (\text{B8})$$

The last term, anti-symmetric in frequency about the mechanical resonance frequency Ω_m , can contribute negatively to the photocurrent spectrum, leading to squeezing below the shot-noise level. The last term may be identified as being due to correlations between the back-action driven motion x_{ba} , and the fluctuations of the transmitted field that set the imprecision in homodyne detection. The above equation is used to fit the squeezing spectrum in Fig. 2 of the main manuscript.

1. Relation to heterodyne sideband asymmetry

Following the discussion of heterodyne detection in Sec. A1, leading up to equations (A21) and (A22), the heterodyne photocurrent spectrum centred around the

intermediate frequency Ω_{IF} is given by,

$$\begin{aligned}\bar{S}_{II}^{\text{het}}(\Omega - \Omega_{\text{IF}}) &\propto \bar{S}_{qq}^{\text{out}}(\Omega) + \bar{S}_{pp}^{\text{out}}(\Omega) \\ &\quad + \text{Im} (S_{qp}^{\text{out}}(-\Omega) - S_{pq}^{\text{out}}(+\Omega)),\end{aligned}\quad (\text{B9})$$

where $\Omega \geq 0$ and the approximation $\Omega_{\text{IF}} \gg \Omega_m \gg 0$ is used. Indeed, the asymmetry in the heterodyne spectrum, about $\Omega = \Omega_{\text{IF}}$, arises from the imaginary part of the quantum correlations between the phase and amplitude of the transmitted field. Compared to the analogous expression for the homodyne photocurrent spectrum in Eq. (B7), where the real part of the correlation leads to optical squeezing, it is the imaginary part of the phase-amplitude correlation (Eq. (B5)) that contributes to sideband asymmetry.

Appendix C: Displacement spectrum of a cold-damped mechanical oscillator

Here we recall a few useful expressions for the displacement spectrum of a cold-damped mechanical oscillator [17, 25]. We denote by x the physical displacement of the oscillator, and by $y_{\text{hom}} = x + x_{\text{imp}}^{\text{hom}}$, the apparent displacement measured at the in-loop (homodyne) detector. Following the arguments detailed in the supplementary information of [17], we get,

$$\begin{aligned} \bar{S}_x(\Omega) = & \underbrace{|\chi_{\text{eff}}(\Omega)|^2 (2n_{\text{tot}} + 1) \bar{S}_x^{\text{zP}}(\Omega_{\text{m}})}_{\bar{S}_x^{\text{tot}}(\Omega)} \\ & + \underbrace{|\chi_{\text{eff}}(\Omega)|^2 (2n_{\text{imp}}^{\text{hom}} g_{\text{fb}}^2) \bar{S}_x^{\text{zP}}(\Omega_{\text{m}})}_{\bar{S}_x^{\text{fb}}(\Omega)} \end{aligned} \quad (\text{C1})$$

for the physical displacement spectrum, and,

$$\begin{aligned} \bar{S}_y^{\text{hom}}(\Omega) = & \underbrace{2n_{\text{imp}}^{\text{hom}} \bar{S}_x^{\text{zP}}(\Omega_{\text{m}})}_{\bar{S}_x^{\text{imp,hom}}(\Omega)} \\ & + \underbrace{|\chi_{\text{eff}}(\Omega)|^2 (2n_{\text{tot}} + 1) \bar{S}_x^{\text{zP}}(\Omega_{\text{m}})}_{\bar{S}_x^{\text{tot}}(\Omega)} \\ & + \underbrace{|\chi_{\text{eff}}(\Omega)|^2 (-2n_{\text{imp}}^{\text{hom}} g_{\text{fb}}) \bar{S}_x^{\text{zP}}(\Omega_{\text{m}})}_{2\text{Re}\bar{S}_{x_{\text{fb}}x_{\text{imp}}}^{\text{hom}}(\Omega)} \end{aligned} \quad (\text{C2})$$

for the apparent displacement spectrum. Here, the effective susceptibility for the displacement is given by,

$$\chi_{\text{eff}} = \frac{\Omega_m \Gamma_m}{(\Omega_m^2 - \Omega^2) + i\Omega(\Gamma_m + \Gamma_{\text{fb}})}, \quad (\text{C3})$$

where $\Gamma_{\text{fb}} = \Gamma_m g_{\text{fb}}$ is the feedback damping rate. In the main text we use the approximation $\Gamma_m + \Gamma_{\text{fb}} \approx \Gamma_{\text{fb}}$.